IAC–24–A3,IP,44,x91140

ENEA: characterization of Near Earth Objects through the development of an asteroid hopping mission

Sarah Aiani[a], Carlos Albiñana Burdiel[b], Alice Balest[c], Giulio Morandi[d], Amanda Sánchez Magris[e], Dario Scimone[f]*, Michèle Lavagna[g]

[a] *MSc student in Space engineering, Politecnico di Milano, sarah.aiani@mail.polimi.it*
[b] *MSc student in Space engineering, Politecnico di Milano, carlos.albinana@mail.polimi.it*
[c] *MSc student in Space engineering, Politecnico di Milano, alice.balest@mail.polimi.it*
[d] *MSc student in Space engineering, Politecnico di Milano, giulio1.morandi@mail.polimi.it*
[e] *MSc student in Space engineering, Politecnico di Milano, amanda.sanchez@mail.polimi.it*
[f] *MSc student in Space engineering, Politecnico di Milano, dario1.scimone@mail.polimi.it*
[g] *Department of Aerospace Science and Techology, Politecnico di Milano, 20156, Milano, Italy, michele.lavagna@polimi.it*
* *Corresponding author*

Abstract

The Exploration of Near Earth Asteroids (ENEA) is a space mission concept developed by a team of eleven MSc students from Politecnico di Milano over five months. ENEA aims to approach three Near Earth Asteroids (NEAs), of particular interest to better understand the Solar System's formation and evolution. Specifically, it intends to determine the gravel size and surface composition of `2006 HZ51` and `2004 QD14` during flybys and map small-scale features, and the internal structure of `2000 SG344`, by rendezvous. The latter is a potentially hazardous asteroid as it ranks fourth on ESA's risk list for Earth collisions, making it a great candidate for a more in-depth study. The targeted asteroids vary significantly, with diameters ranging from only 40 m to 400 m and orbit with eccentricities and inclinations from 0.06 to 0.45 and 0.11 deg to 12.4 deg, respectively, presenting unique challenges for mission analysis design. Starting from state-of-the-art research and statistical studies, a trade-off between different architectures was performed to limit the available solutions regarding the number of spacecraft and propulsion. Given the characteristics of the small objects under study, a thorough analysis of the payloads was performed to comprehend their effect on the mission design. Using the concurrent engineering methodology, with each student in charge of one subsystem, the mission development was addressed in an iterative process to enforce subsystem interaction and cooperation. A common design model, guided by mission objectives and requirements, led to the proposal of a singular spacecraft. ENEA would begin with the first interplanetary leg to reach `2006 HZ51`; the spacecraft would then enter the second transfer leg to `2004 QD14`. The two NEAs would be flown by while scientific data is retrieved. After the third interplanetary transfer, two years after launch, the spacecraft would rendezvous with `2000 SG344`. The last and smallest NEA would be studied in two stages: in the first one, the spacecraft would map the surface of the target ranging from 100 km to 500 m of distance from it, while in the second one, it would perform a radio science experiment on a quiescent terminator orbit at 120 m of altitude. Lastly, the spacecraft would be set to crash into `2000 SG344` or proceed to a graveyard orbit in compliance with Planetary Protection Guidelines. The paper presents the subsystem specifications, mission architecture, criticalities and technology needed to improve the mission concept. Despite the stringent constraints and high uncertainties, the ENEA design has proven to produce feasible results in achieving the scientific requirements.

1. Introduction

ENEA is a space mission concept, developed by a team of eleven Politecnico di Milano students, to study the global physical properties of three Near Earth Asteroids in different size regimes.

Our Solar System hosts thousands of small objects of different shapes, volumes, and compositions, orbiting in numerous regions. The ones in close proximity to Earth, the so-called Near Earth Objects (NEOs), are of particular interest since they provide useful data to better understand the solar system's formation and evolution. Moreover, these objects can pose serious threats to our planet due to their peculiar orbital parameters. For this reason, having enough data to plan and execute planetary defense missions is crucial. In this regard, this mission is developed to answer critical questions about asteroids `2006 HZ51`, `2004 QD14` and `2000 SG344`. ENEA objectives are:

- determine the gravel size and surface composition of `2006 HZ51` and `2004 QD14` during flybys
- map small-scale features and internal structure of `2000 SG344` by rendezvous

In addition, the spacecraft shall stay below 500 kg of wet mass and provide a resolution of 1 m/px during flybys and in the order of 1 cm/px during rendezvous. Finally, the launch date shall be before 2030. The characteristics of the three NEOs are summarized in Table 1. The mission's drivers are mainly the mass and the Technology Readiness Level (TRL). The first derives directly from the mission requirements, while the second comes as a consequence of the stringent launch date.

In the following sections, a preliminary study of the mission is presented. The design starts with the study of the state of the art and the modeling of the environment that will be encountered. This information, together with an in-depth analysis of the payload needed to fulfill the scientific requirement, is used to choose the overall architecture of the spacecraft. In the final section, the modeling of the different subsystems is presented.

2. State of the Art

Over the past decades, there have been several missions to observe asteroids. The outcomes of those efforts expanded the knowledge of the early formation of the Solar System, and tested techniques for Earth's planetary defense. This chapter explores the current state of the art for asteroid missions, focusing on the most significant ones, listed in Table 2.

Table 2. Asteroid Missions

Mission	Target
Hera	Dydimos, Dimorphos
Psyche	Psyche
NEA scout	2020 GE
DART	Dimorphos
OSIRIS-REx	Bennu
Hayabusa-2	Ryugu
Rosetta	Churyumov Gerasimenko
Hayabusa	Itokawa
NEAR	EROS

Although directed to targets different in shape, composition, and distance from the Sun, the missions mentioned in Table 2 are considered references for the ENEA mission design because of the similar environment. In Table 3 is reported an overview of the different missions' targets.

Except for NEA Scout, which failed, no missions can be identified that have visited asteroids smaller than 100 m in diameter. However, it is possible to identify those that observed a target at a distance from the Sun similar to the one of ENEA. They are: Hera, OSIRIS-REx, Hayabusa, Hayabusa-2 and NEAR.

Table 3. Target's characteristics

Target	Diameter	Mass
Dydimos	765 m	$5.2{\cdot}10^{11}$ kg
Dimorphos	160 m	$1.33{\cdot}10^{9}$ kg
Psyche	$250{\cdot}10^{3}$ m	$2.72{\cdot}10^{19}$ kg
2020 GE	11 m	$\sim$
Bennu	> 200 m	$7.8{\cdot}10^{10}$ kg
Ryugu	896 m	$4.5{\cdot}10^{11}$ kg
Itokawa	330 m	$3.51{\cdot}10^{10}$ kg
Eros	$16.84{\cdot}10^{3}$ m	$6.687{\cdot}10^{15}$ kg

Since these missions explore unknown objects, they are designed to collect and process data about their target, to then use it to plan the next step.
All the cited missions follow a procedure for their proximity operations similar to the following: once the spacecraft reaches the target, it settles on a distant orbit where it spends some time characterizing the asteroid, using the collected data to update the gravity potential model and the surface properties. Then, it moves to a lower orbit and repeats the process until the desired accuracy is achieved.

2.1 Guidance & Navigation

Due to the mission's nature and targets' uncertainties, guidance and close proximity navigation are critical. In this section, some of the new technologies that were devel-

Table 1. Target asteroids' characteristics

NEO	HZ51	QD14	SG344
Diameter	410 ± 90 m	143 -24/+49 m	40 -25/+30 m
Albedo	0.42 ± 0.23	0.37 -0.18/+0.20	-
Orbital parameters	i = 12.4°; e = 0.45; a = 1.895 AU	i = 6.2°; e = 0.338; a = 0.94 AU	i = 0.11°; e = 0.067; a = 0.975 AU

oped for three of the previously mentioned missions are presented:

- For OSIRIS-REx, one of the most significant flight system technologies is the Laser Imaging Detection and Ranging (LIDAR) sensor, which was developed and used as the main instrument for supporting proximity navigation and Touch and Go operations. A Natural Features Tracking (NFT) program was also added to improve the system's reliability, acting as a fully autonomous backup to the LIDAR. NFT uses two redundant optical cameras and an internally developed software to look for known features on the asteroid's surface, for navigation purposes [1]
- The DART mission tested several innovative technologies, including a new completely autonomous guidance system, the APL-developed Small-body Maneuvering Autonomous Real-Time Navigation (SMART nav) algorithm. SMART nav works in synergy with its payload Didymos Reconnaissance and Asteroid Camera for Optical navigation (DRACO) to autonomously identify and distinguish Didymos and Dimorphos, and independently direct and maneuver the spacecraft [2]
- The Hayabusa mission was also supposed to have an autonomous guidance system for proximity operations; however, due to the highly irregular shape of the target, the optical navigation system was not capable of precisely tracking the asteroid; therefore, the team opted for an alternative solution based on terrain recognition in quasi-real time. When the spacecraft made its initial approach, it jettisoned a marker that served as an artificial landmark. The primary purpose of the target marker was to enable the spacecraft to autonomously identify lateral velocity, critical for landing [3]

3. Environment

The radiation environment of the mission can be divided into two parts: inside Earth's magnetosphere and deep space. For the first one, the most relevant radiation types are trapped protons and electrons in the Van Allen belts. Since ENEA is a deep space mission, the amount of time spent in the magnetosphere will be brief compared to the duration of the mission, therefore, the dose of this type of radiation can be neglected in the preliminary analysis. On the other hand, radiation in deep space mostly comes from the Sun's energetic particles and Galactic Cosmic Rays (GCR). To calculate the thickness of the aluminum plate, needed to shield said particles, the CREME96 [4] model is implemented. This data is used later on by the subsystem to design the shielding mechanism if needed.

In regards to the thermal environment, the heat flux from the asteroids has great uncertainties due to the low precision of the albedo measurements and surface absorptivity. Solar and albedo heat fluxes for the three asteroids are computed to account for the close approach phases, at a distance between 10 km and 20 km from the asteroids' surface. The two largest asteroids, `2006 HZ51` and `2004 QD14`, have more elliptical orbits; for this reason, solar heat flux and albedo heat flux near those objects fluctuate between perihelion and aphelion. Concerning the infrared heat flux generated by each of the three asteroids, its behavior is strongly related to the temperature of the external surface. As the only thermal property known is the albedo coefficient, a range of surface temperatures between 200 K and 400 K [5], and an average value of the emissivity coefficient equal to 0.9 [6] are assumed.

From the model, it is possible to notice that the main source of thermal loads is the solar heat flux, while albedo and infrared heat flux can be neglected. This is due to the limited extension of the asteroids' surface, and the difference in orders of magnitude between the spacecraft-asteroid distance and the radius of the object.

Since `2006 HZ51`,`2004 QD14` and `2000 SG344` have not been studied, there is no precise data about the magnitude of their gravity field. Moreover, apart from the diameter mean values, information about elongation and shape is not provided, the same holds for the precise mass and sizes of the objects. Therefore, to determine the asteroids' gravity field, a parametric model must be implemented to understand the influence of these properties.

For a preliminary estimate of the gravity field, the Triaxial Ellipsoid model is used [7] on a body with the same mean diameter as asteroid `2006 HZ51`, which is the biggest one. The average density is taken as 1.38 g/cm^3 [8], assuming it is a carbonaceous-like asteroid with properties similar to Ryugu. First, the magnitude of the gravity field is computed for both an oblate and an elongated geometry. These calculations result in a gravitational acceleration in the order of 10^-5 m/s^2 up to a kilometer over the asteroid's surface. Therefore, its effect on the spacecraft can be neglected.

Data from the Space Weather Prediction Center and the US National Oceanic and Atmospheric Administration shows that in 2025, a peak in solar activity is predicted. This event can cause telecommunications failure, degradation of materials, darkening of lenses and cameras, and reduction of solar array power generation. After 2026 the solar activity trend decreases. So, given the current launch date of December 2026, the ENEA mission will not take place on a solar activity maxima.

4. Payloads & Scientific Return

To achieve ENEA's mission objectives, the spacecraft hosts onboard a set of scientific instruments: a series of imagers and a spectrometer. The science traceability matrix, in Table 4, reports their usage and expected products.

It should also be noted that, through radio science, the Tracking Telemetry and Telecommand (TTMTC) subsystem is used for scientific purposes. The activities are categorized as:

- **Radio science**: ground stations are used to precisely reconstruct the state of the spacecraft when in close proximity with the target. These measurements are then processed to produce a model of the asteroid's gravity potential. The experiment is carried out during a quiescent period, in which there are no maneuvers, including desaturation ones. This period should be as long as possible to maximize the amount of data collected, with the ground track covering as much surface of the target as possible. The activity is carried out in different steps, each closer to the asteroid, in order to refine its gravitational model at each phase [9]

- **Spectrometry**: the surface composition of the targets is characterized by measuring the spectral energy distribution of the radiation emitted by the body. In particular, x-rays are reflected by some elements when excited by solar radiation. γ-rays are emitted by radioactive atoms and by some elements when excited by GCR

- **Optical measurements**: the shape and volume of the targets are reconstructed using photochilometry technique, using both object shading and lighting direction to produce a geophysical model of the asteroid. The sub-products of this technique are maps of elevation, slope, roughness, and surface tilt with respect to the spacecraft position vector [10]. Moreover, optical sensors are suitable for tracking small-scale features present on the surface of the body [11]

4.1 Imagers

Two panchromatic cameras are hosted onboard, both sharing the same type of sensor - 5.5 μm pixel size with 10-bit radiometric precision. They differ in Field of View (FoV) and sensor size, the first one has a wide 5.5 deg FoV with a 2048x1088 px size, while the second one is a narrow 1.7x2.2 deg FoV 4096x3072 px. Their properties, alongside scientific requirements, highly influence the mission design. For this reason, a comprehensive study is performed to define the boundaries of operations applied to this specific case, and the constraints imposed on trajectory and subsystem design.

At first, the boundaries of operations are defined in terms of distance from the targets (h) in the three science periods: flyby one, flyby two, and rendezvous. Using a pinhole model, the Ground Sampling Distance (GSD) is parameterized as a function of h. Subsequently, an optical analysis is performed to verify that the optical resolution is always higher than the needed geometrical one. This means that both cameras are capable of resolving the image without the superimposition of two diffraction peaks inside the same pixel, for any given distance from the target. Table 5 provides the outputs of the process.

For flybys, only the narrow camera guarantees enough performance to meet requirements and perform the closest approach at a safe distance. Notably, for almost all ranges, the target is entirely inside the field of view. For rendezvous instead, the lower boundary is due to the focusing capability of the sensors - 400 m for the wide camera, 10 km for the narrow one - and both instruments can be used according to the acquisition distance. It should be noticed that, due to trajectory control limitations, the upper boundary for the narrow camera at rendezvous is relaxed to 16 km, allowing the acquisition of scientifically meaningful images at a slightly lower resolution.

To obtain the available science time, the spacecraft is as-

Table 4. Science traceability matrix of ENEA mission

Scientific Objective	**High Level Products**	**Contributing Payloads**	**Mission Phase**
Target's mass and gravity harmonics estimation	Target shape, volume, large-scale structures	Optical sensors, TTMTC, retroreflector (if any)	Flyby, rendezvous
Surface mapping and characterization	Maps of elevation, slope, roughness, gravel size distribution, and surface composition	Optical sensors, spectrometer	Flyby, rendezvous
Target's internal structure and small-scale features mapping	Maps of elevation, slope, roughness, gravel size distribution, and surface composition	Optical sensors, spectrometer	Rendezvous

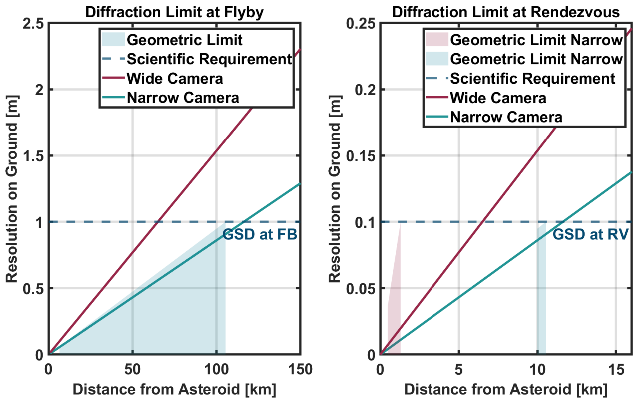

Fig. 1. Optical resolution during rendezvous

sumed to be moving on a linear trajectory with respect to the target, Eq. (1) gives $t_{science}$ as a function of the closest approach distance (r_p), while the maximum distance required to comply with the 1 m/px is set to 105 km.

$$t_{science} = 2 \cdot \frac{\sqrt{105^2 - r_p^2}}{v_{sc}} \qquad [1]$$

An iterative process is then performed to find a feasible r_p both from Attitude Determination and Control Subsystem (ADCS) and Mission Analysis (MA) viewpoints. Given the high approach velocities, the slew rate that the actuators shall provide to meet scientific requirements is a critical aspect. By setting a maximum rate of 6 deg/s and the closest approach distances of 80 km and 95 km the first and second flyby, respectively, the resulting science time is 16 s for flyby one and 9 s for flyby two.

To avoid blurry images, the blur ratio defined as $br = \Delta S/GSD$ shall be less than 0.5 - taking into account the time for the camera shutter to open and close. Only the first flyby poses a constraint on the required speed. For flyby two, given the reduced dimensions of `QD14`, even a very low acquisition speed can be used. The Frames Per Second (FPS) are set to 17 images per second for both cases, implying a shutter speed of 29.3 ms.

During the rendezvous, instead, given the reduced relative velocity and the peculiar shape of the trajectory no criticality is present in terms of motion blur or acquisition frequency. A value of 1 FPS is deemed enough to acquire the images for both cameras.

4.2 Spectrometer

The analysis of the payload suite is completed by evaluating spectrometer performances, taking as baseline the instrument flown onboard NEAR mission [12].

Given the nature of the physical process to study, an x-γ-ray spectrometer has the following limitations:

- Emission of x-rays from asteroid surface elements is highly influenced by the amount of solar radiation received. Therefore, the scientific return is directly dependent on the distance from the Sun at which the flybys and the rendezvous take place, as well as the current solar activity

- Emission of γ-rays is instead decoupled from solar activity. Moreover, γ-rays are weaker in power, meaning that high FoVs and long exposure times are needed

Additionally, the effect of the space environment - mainly radiation - can affect the quality of data production. Given the criticalities described and the difficulty in modeling the behavior of such an instrument, the solution adopted is to activate it as soon as the science phase starts for all three cases.

4.3 Adopted Strategy

Based on the performed analysis, a series of considerations can be derived for the payloads. Firstly, during both flybys, only the narrow FoV camera fulfills scientific requirements at a distance compatible with MA and ADCS needs. Moreover, in those two phases, it is unclear whether the spectrometer has enough time to provide sufficient data about the chemical composition of the targets' surface. For this reason, as a preliminary assumption, the instrument is considered active. During rendezvous, instead, all instruments are expected to operate and provide data according to the designed phases.

Table 5. Operational distance ranges for both cameras

Phase	**Narrow Cam**	**Wide Cam**
First Flyby	17 km < h < 105 km	6 km < h < 13 km
Second Flyby	5.8 km < h < 105 km	1.9 km < h < 12.8 km
Rendezvous	10 km < h < 10.5 km	0.4 km < h < 1.3 km

5. Architecture

The architecture, at the system level, is highly influenced by two aspects: the asteroid-visiting strategy and the propulsion technology. For the former, three options are identified:

- **Single Spacecraft**: this is the most basic procedure from the operation and hardware point of view. The satellite performs both flybys and arrives at the final rendezvous point
- **Mothership**: a larger spacecraft carries two smaller satellites. These detach from the mothership and get closer to the flyby asteroids, at a lower relative velocity. This solution grants more time to perform science with the required ground resolution. A larger scientific return is obtained, at the cost of higher operative and hardware costs
- **Twin Spacecrafts**: the mission is split in half by using two spacecraft. There are two options for this approach. *Option 1*: one satellite performs a flyby and the final rendezvous, with the other satellite performing the flyby on the other asteroid. *Option 2:* one spacecraft performs both flybys, while the other directly arrives at the rendezvous asteroid

On the other hand, two main propulsion approaches are studied, for the primary propulsion system:

- **Continuous Thrust**: maneuvers and cruise propulsion are performed using a thrust level in the N-mN range. This approach yields less mass of propellant for the same value of ΔV with respect to the impulsive option
- **Impulsive Thrust**: maneuvers and cruise propulsion are performed at a higher thrust level and can be assumed to be impulsive. These systems reduce the power budget

Even though the above options are all valid, the combinations including impulsive thrust and/or twin spacecraft are eliminated due to the weight limitation of the mission. A trade-off analysis of the architectures is done using Figures of Merit (FoM). The different parameters are then normalized in a scoring system with their respective weight, obtaining a final score as a weighted sum.

FoM are mission-critical parameters that influence the choice of the final architecture. A scoring system from one to three is given to each FoM (lower is worse). The ones identified for the ENEA mission are:

- **Power budget**: index of the total power required by the spacecraft. This mainly impacts the size of the solar panels. Larger solar panels increase hardware complexity due to the need for larger deploying mechanisms, especially when considering the contingency and safety margins for power. Therefore, a larger power requirement negatively impacts the trade-off analysis.
  1. Very large power demand, must use multiple/stacked deployable solar arrays and have strict control on Sun eclipses
  2. Large power demand, must have deployable solar panels
  3. Lower power demand, no need for deployable arrays
- **Mission lifetime**: a longer mission lifetime increases material degradation and the failure probability of components. The difference in mission lifetime is derived from the times of flight (ToF). Thus, a larger ToF scores negatively in the trade-off analysis.
  1. Mission lifetime exceeds the 5-year mark
  2. Mission lifetime is no larger than 5 years
  3. Mission lifetime does not exceed the 2-year mark
- **Scientific return**: this figure is paramount to satisfy the mission objectives. It is measured as how much data the mission can retrieve and its relative quality. In this sense, closer images of the asteroid's surface with greater ground resolution are better than pictures taken from further away.
  1. The expected scientific data complies with the minimum requirements of the mission
  2. Expected large amount of data compiled on the science objectives
  3. Expected scientific data goes beyond the basic science requirements
- **Complexity**: given by the number of assemblies, components, and interfaces that make up the system and their respective production difficulty.
  1. Architecture requires special considerations in material selection and interfaces, and has complex moving mechanisms that are critical for the outcome of the mission
  2. Architecture requires special considerations in material selection and interfaces, or has complex moving mechanisms that are critical for the outcome of the mission
  3. Architecture needs no complex moving parts, interfaces, or special considerations in material selection and subsystem allocation

Each FoM has an associated weight to measure its relative importance within the architecture selection. These are seen in Table 6.

Table 6. FoM and weight assigned for each

Figure Of Merit	Weight	Weight%
Power Budget	2	13 %
Mission Lifetime	1	6 %
Scientific Return	8	50 %
Complexity	5	31 %

The two main architecture candidates are compared in Table 7 and Table 8. The single spacecraft architecture is the best option for the ENEA mission.

Table 7. Score: single spacecraft + continuous thrust

Figure Of Merit	Score	Weighted score
Power Budget	2	0.25
Mission Lifetime	3	0.19
Scientific Return	1	0.5
Complexity	3	0.94
Final Score		**1.88**

Table 8. Score: mothership + continuous thrust

Figure Of Merit	Score	Weighted score
Power Budget	1	0.13
Mission Lifetime	3	0.19
Scientific Return	2	0.5
Complexity	1	0.31
Final Score		**1.63**

6. Mission timeline

With a 2026 launch and an expected two-year duration, the mission timeline is presented below.

- **Launch:** 10th December 2026
- **Early Operation Phase & Commissioning:** Payload calibration after 5 days pointing at the Moon
- **1st Interplanetary Leg:** Duration of 5 months
- **2006 HZ51 Flyby:** Closest approach in June 20th 2027 at 85 km
- **2nd Interplanetary Leg:** Duration of 7 months
- **2004 QD14 Flyby:** Closest approach in December 14th 2027 at 95 km
- **3rd Interplanetary Leg:** Duration of 11 months
- **2000 SG344 Rendezvous:** Arrival on the 9th November 2028.
- **Decommissioning & End Of Life (EOL):** Crash on `2000 SG344`

Given `2000 SG344`'s classification as potentially hazardous, the option of leaving the spacecraft in its orbit, after the completion of the mission, is not admissible. The most viable solution entails intentionally directing ENEA to impact the surface of the asteroid.

7. Mission Design

7.1 Mission Analysis

The chosen mission analysis design consists on the implementation of an optimization algorithm aimed at finding an efficient trajectory to visit the three asteroids in the following sequence: `2006 HZ51`, `2004 QD14` and `2000 SG344`. The objective is to minimize propellant consumption while obtaining a feasible trajectory. The three segments - departure to the first flyby, first flyby to the second flyby, and second flyby to rendezvous - are optimized using an indirect method with homotopic approach [13][14].

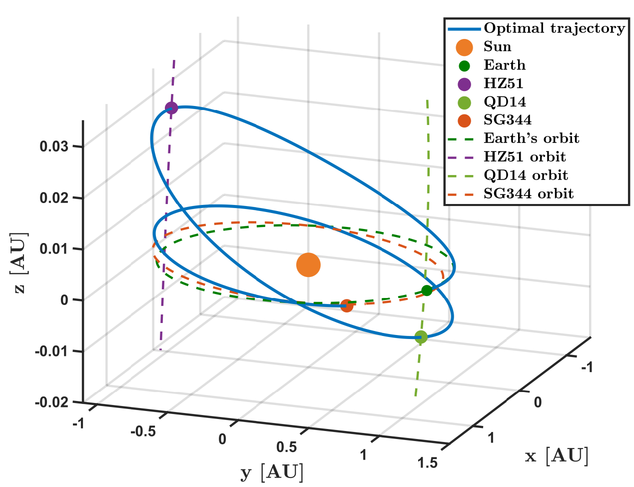

Fig. 2. Interplanetary trajectory

The trajectory design focuses on encountering the asteroids at their nodal points, as can be seen in Fig. 2, limiting propellant allocation for plane change maneuvers. Furthermore, on the optimized path, the spacecraft maintains a maximum distance from the Earth of less than 0.2 AU and a maximum distance from the Sun of less than 1.1 AU, benefiting TTMTC, the Electric Power Subsystem (EPS), and Thermal Control Subsystem (TCS) design.

The trajectory allows the spacecraft to face the illuminated side of the asteroids at close approach during flybys. The distance from the targets and the encounters' relative speeds comply with the resolution needs of the payload and dynamics of the ADCS.

7.2 Guidance, navigation & control

The main drivers for the design of the Guidance, Navigation & Control (GNC) subsystem are the science requirements for the rendezvous phase: to be close enough to the asteroid to acquire images with the given resolution and to determine the gravity properties of the asteroid.

Due to the lack of information on the third asteroid, it is assumed to have a North Pole direction rotational axis and a retrograde rotation in an ecliptic reference frame. Moreover, the asteroid is modeled as a sphere with uniform mass, Table 9 compiles the values used as references.

The model of the motion is implemented with the use of forced orbits, whose characteristics can be designed to suit the needs of the mission. Secondary thrusters are used to perform station-keeping maneuvers and to target specific trajectories. Two differential correction schemes are executed, one to aim the desired trajectories, and the other for station keeping at holding points.

The operation around `2000 SG344` is split into two distinct science stages. The first stage will map the surface, while the second, at a closer distance, will perform the radio science experiment. The former stage consists of three phases:

- *Holding point A*: placed at 100 km on the trailing side of the in-track direction along increasing true anomaly, where the orbital period and spin axis of the asteroid are estimated
- *Holding point B*: on the radial direction between the Sun and the asteroid (R-bar), at 15 km from the latter, where images can be taken with the best illumination conditions
- *Rhomboidal orbit*: centered around a point on the R-bar distant 500 m from the surface of `2000 SG344`, where more images can be taken with varying illumination conditions and different angles

At each corner of the rhomboidal orbit shown in Fig. 3, the secondary thrusters change the spacecraft's trajectory to follow the orbit's shape. Since, at this distance, the gravity of `2000 SG344` is too weak to establish an orbit. Moreover, by following this trajectory, the same subject can be photographed in different lighting conditions.

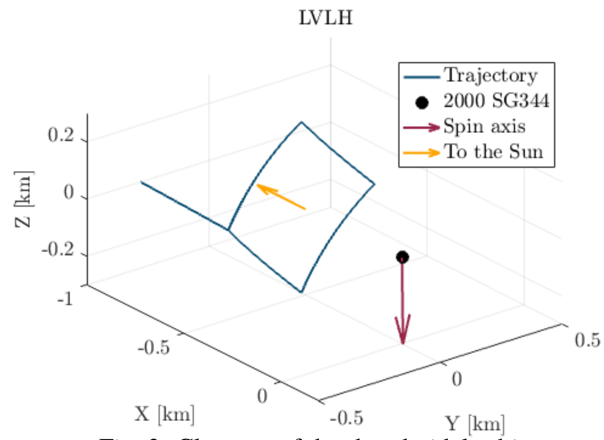

Fig. 3. Close-up of the rhomboidal orbit

The gravitational properties of `2000 SG344` are measured through a radio science experiment. It consists of tracking the trajectory of the spacecraft while it follows a quiescent orbit[*] around the asteroid. The spacecraft is placed on a 120 m altitude terminator orbit, shown in Fig. 4, to reduce the disturbing effects of the solar radiation pressure. While orbiting, it is continuously tracked from Earth and the data collected is then used to estimate the gravitational properties of `2000 SG344`.

[*] A quiescent orbit is an orbit where no orbital or attitude maneuvers are executed

Table 9. Physical parameters of `2000 SG344` [15]

	Mass	**Diameter**	**Radius of SOI**
Nominal value	7×10^7 kg	40 m	154 m
Uncertainty	$[2.33 \times 10^7, 21 \times 10^7]$ kg	$[18, 80]$ m	$[99, 239]$ m

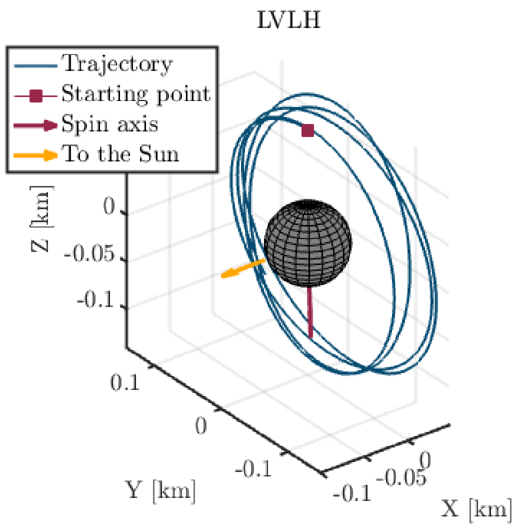

Fig. 4. Quiescent orbit

The ΔV budget of the proposed trajectory design is presented in Table 10. A margin of 100% is applied to ensure a flexible design.

Table 10. ΔV budget of rendezvous phase

Phase	ΔV
HPA	0.474 m/s
HPB	0.693 m/s
Rhombus	0.469 m/s
Total	1.636 m/s
Margin	100%
Total with margin	3.272 m/s

7.3 Attitude determination & control

The most demanding phases of the mission in terms of attitude determination and attitude control are the flybys. The spacecraft executes a rotation of about 180 degrees around the z-body axis in less than one minute while satisfying the pointing accuracy required by scientific payloads. For these reasons, the two main drivers that dictate the choice of the architecture of the subsystem are the high level of torque needed to slew the spacecraft and the pointing accuracy at the flybys.

Table 11 and Table 12 compile the subsystem architecture in terms of actuators and sensors, respectively.

Table 11. Subsystem architecture - actuators

Actuators	Number
CMGs	4 (1 redundant)
RCTs	12 (4 redundant)

Table 12. Subsystem architecture - sensors

Sensor	Number
Star Trackers	2
IMUs	2 (1 redundant)
Fine Sun Sensors	5
Coarse Sun Sensors	2
Navigation Cameras	4 (2 redundant)

Four Control Moment Gyroscopes (CMGs), placed in pyramidal configuration are selected as primary actuators. Twelve reaction control thrusters are needed to execute the de-tumbling maneuvers and large slews with a lower pointing accuracy.

During the closest approach with the asteroids, the attitude determination cannot rely on the star trackers because the spacecraft's angular velocity is higher than the maximum operative speed allowed by the sensor. To maintain a low absolute knowledge error, the measurements coming from fine-spinning Sun sensors and Inertia Measurement Units (IMUs) are integrated with navigation cameras that localize the center of brightness of the asteroid.

A three-axis stabilization is selected for all the mission phases. Five control modes cover all the operational tasks required for the ADCS:

- *Sun Acquisition Control Mode (SACM)*: performs the first attitude acquisition, the de-tumbling maneuver, and the solar array deployment
- *Safe Hold Control Mode (SHCM)*: mode in which the spacecraft can enter any mission phase when a safe attitude is required to solve anomalies or criticalities
- *Coarse Control Mode (CCM)*: used to start acquiring the target inside the FoV of the cameras and to realign the x-body axis towards the velocity vector
- *Fine Control Mode (FCM)*: used during the flybys and the close observation phase. The spacecraft enters this mode also during the commissioning phase to check the scientific instruments

- *Stand-By Control Mode (SBYCM)*: is a hibernation mode to preserve resources and to counteract external and internal disturbances during long cruise phases

Table 13 shows the modes to use for each mission phase.

Table 13. ADCS modes and control strategy

Mission Phases	Control Modes
LEOP	SACM, SHCM
Commissioning	CCM, FCM, SHCM
Cruise 1	SBYCM, SHCM
Flyby 1	CCM, FCM, SHCM
Cruise 2	SBYCM, SHCM
Flyby 2	CCM, FCM, SHCM
Cruise 3	SBYCM, SHCM
Rendezvous	CCM, SHCM
Global Obs.	SBYCM, SHCM
Close Obs.	CCM, FCM, SHCM
Disposal	N/A

7.4 Propulsion

Given the constraints on the mass as well as the early launch date of the mission, the Propulsion Subsystem (PS) needs to use thrusters with a high specific impulse and TRL. For this reason, the ion thruster is selected as the main engine of the spacecraft. Since the mission does not have a particularly high request of performance, flight-proven off-the-shelf components can be selected; therefore guaranteeing a high TRL.

To ensure the needed thrust, four ion thrusters are used, their characteristics are shown in Table 14.

Table 14. Primary thrusters

Propellant	Xe
Isp	1700 s
Thrust	25 mN
Power	825 W

A high-pressure flow control unit is chosen to guarantee the correct feeding of the engine since Xenon must be pressurized at 80 bar before launch. For this same reason, adding a pressurization system to the primary propulsion system is unnecessary. Finally, two Power Processing Units (PPUs) are connected to two engines each to guarantee a minimum thrust level even in case of failures.

To be able to complete the mission objectives, a secondary propulsion system is added to be used for GNC and ADCS purposes. Given that these subsystems require a high-thrust impulsive response, and to contain the mass of the overall system, bipropellant thrusters are implemented. The engine's characteristics are presented in Table 15.

Table 15. Secondary thrusters

Propellant	MMH and NTO
Isp	292 s
Thrust	10 N
Power	40 W

To ensure responsive control over the three main axes of the spacecraft, twelve thrusters are used, accompanied by a pressure-fed system using Helium.

Table 16 and Table 17 compile the mass and power budget of the propulsion subsystem.

Table 16. Budget for the primary propulsion subsystem

Engine	Ion Thruster
Dry mass	71.62 kg
Propellant mass	56.49 kg
Wet mass	128.11 kg
Power	3300 W

Table 17. Budget for the secondary propulsion subsystem

Engine	Bipropellant
Dry mass	5.57 kg
Propellant mass	1.24 kg
Wet mass	6.81 kg
Power	160 W

7.5 Tracking, telemetry & telecommunication

The TTMTC subsystem is engineered to balance low mass and power use, with the ability to send data efficiently across distances up to 0.2 AU.

It uses the X-Band for communication, with data being sent through QPSK modulation and protected by a concatenated code for reliability. The European Space Agency's Deep Space Network is then taken as a reference for the ground segment.

The architecture features two solid state power amplifiers acting in cold redundancy, a 26 dBi medium gain horn antenna inspired by the Rosetta mission and mounted on a 2-axis gimbal for precise aiming, two low gain antennas for omnidirectional coverage, a radio frequency distribution unit, and two transponders acting in hot redundancy during reception and in cold during transmission. The system achieves a data rate of 28 kbps and completes science data downlink in 20 hours.

7.6 Thermal control

The mass constraint requires the thermal control subsystem to be designed primarily to minimize both mass and power consumption. This objective is achieved through the implementation of mainly passive control solutions.

The thermal study is performed by considering the main body of the spacecraft and its solar arrays as thermally decoupled. While the solar arrays are analyzed as a mononode, the main body is studied with a multi-nodal analysis where the nodes are chosen with a trade-off between stringent operative temperature ranges and the amount of dissipated heat power.

The main contributor to the mission's thermal environment is the Sun's heat flux, together with the dissipated internal power. To carry out the design, steady state analysis of the worst hot case (WHC) and worst cold case (WCC) are executed. Table 18 compiles the modes or phases considered for the study.

Table 18. Modes or phases considered for thermal analysis

	WHC	**WCC**
Main Body	Science communication	Safe mode
Solar arrays	Closest to the Sun	Furthest to the Sun

As a result, the main body is externally covered by a multi-layer insulator made of 15 layers of aluminized Kapton, while the inside is painted with black paint. A radiator, taped with silvered FEP Teflon, of 1.15 m^2 is needed to dissipate heat. However, to limit the heat dispersion and the electric power needed for heaters in the cold case, the radiators are covered with passive louvers with the internal surface of the panels covered with Kapton tape. Two heaters, in cold redundancy, provide 80 W of heat power needed to keep the propellant tanks within their operative temperature range. Aluminum-cabled thermal straps connected to the radiator allow the PPUs and CMGs to enhance their heat dissipation.

Table 19 compiles the materials chosen for the main body and their properties.

Table 19. Main body materials' optical properties

Material	α	ϵ
MLI [16]	0.14	0.05
Black paint [17]	0.95	0.85
Kapton tape [17]	0.38	0.67
Silvered FEP Teflon tape [17]	0.09	0.88

The solar arrays do not need thermal control solutions. They are covered by white paint on their shadowed side and by cover glass on top of the solar cells on their sunlit side. Table 20 compiles the properties of the materials chosen.

Table 20. Solar arrays' optical properties

Material	α	ϵ
Cover glass [18]	0.9	0.88
White paint [17]	0.3	0.85

7.7 Electric power

The spacecraft's primary energy source comprises two solar panels with a total area of 22.3 m^2, sized to meet the power requirements of the most demanding mode, $\sim$4832 W at 1.065 AU from the Sun. Table 21 compiles the higher power request of the overall system.

Table 21. Science Communication mode, power requirements at subsystem level

Subsystem	**Power**
Payload	9 W
Thermal Control	OFF
Power	97 W
TTMTC	52.5 W
On-board data handling	70 W
ADCS	307.4 W
Propulsion	3491 W
Total	4027 W
Total + 20% margin	4832.4 W

The design follows a worst-case scenario approach that considers: End Of Life (EOL) degradation due to radiation damage, the highest temperature reached throughout the mission by the Solar Array, and two strings failure - one for each wing. A Solar Array Drive Assembly (SADA) is needed to keep the panels pointed toward the Sun during the cruise phase, allowing to meet the high power demand without requiring oversized solar panels. The SADA is also crucial for flyby operations as the possibility of fully rotating the panels allows to minimize the use of the secondary batteries, hence reducing their mass.

The secondary energy source is an 820 Wh Li-Ion battery sized to ensure roughly 50 minutes of autonomy during flyby operation, considering a single-string failure. As no eclipses are foreseen during any of the mission phases, it is assumed that the battery will only be needed for de-tumbling and flyby operations.

7.8 Configuration

The spacecraft's configuration is driven by subsystem requirements and constrained by the selected launcher. In this regard, the Falcon 9 is chosen as launcher baseline due to its availability, launch readiness, and performance. Its fairing provides enough volume to fit any shape in this class of spacecraft. As for the solar panels, due to their large surface, a launch configuration compatible with structural loads needs to be implemented, for this reason, a deployable solution is selected.

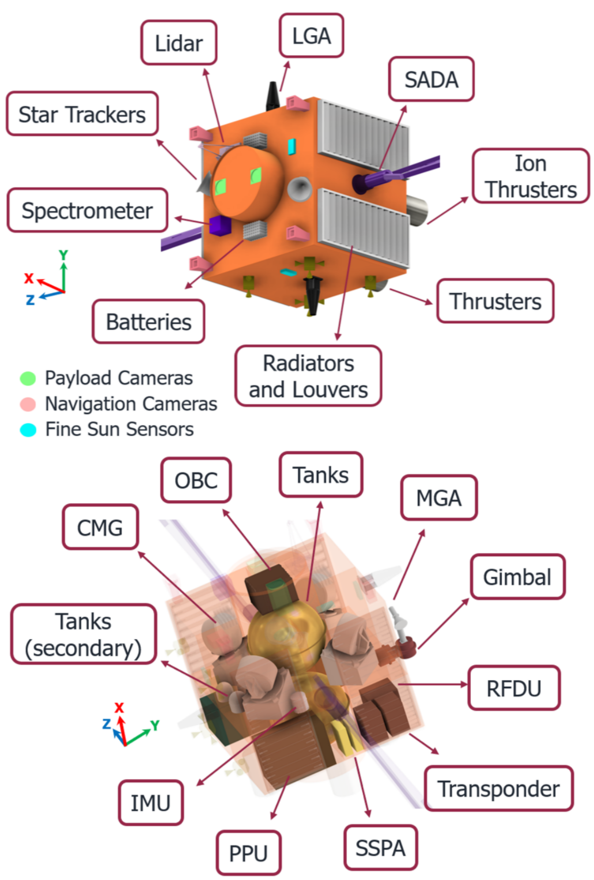

Fig. 5. Components placement

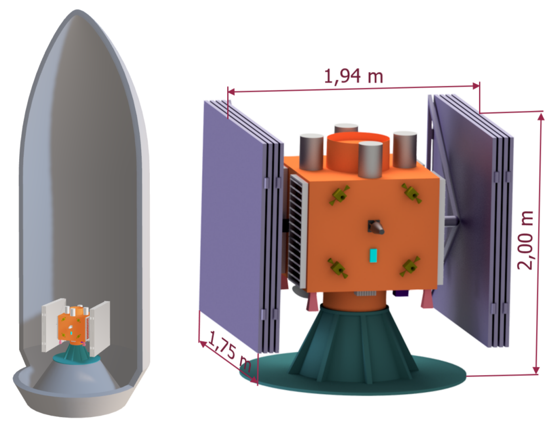

Fig. 6. Fairing and stowed spacecraft

Figure 6 shows the stowed configuration inside the launcher's fairing, together with the launch adapter which does not detach at spacecraft separation.

Based on ADCS requirements, internal components are placed to reduce the inertia about the z-axis as much as possible to satisfy the attitude control strategy. Another important constraint is placing the navigation cameras along the pointing direction (x-axis), opposite the thrusters, to avoid plume impingement. Figure 5 shows the internal displacement of the subsystems' main components.

8. Mass breakdown

The mass budget of the discussed spacecraft is present in Table 22. These numbers include the margins stated by the ESA [19].

As can be seen, the total wet mass is higher than the 500 kg requirement. In this regard, the subsystems with a higher mass (EPS, PS, ADCS, and structure(STR)), are expected to sustain a reduction, if a more refined MA study with lower thrust or a new flyby approach is found.

9. Conclusions

ENEA mission plans to flyby with asteroids 2006 `HZ51` and 2004 `QD14`, and rendezvous with 2000 `SG344`, studying their global physical properties and surface features to advance the scientific knowledge on potentially hazardous Near Earth Objects. The obtained solution is a single spacecraft of 525.99 kg. The performed analysis shows that the mission is feasible and the scientific goals are achievable. However, two criticalities must be addressed in later phases of the design process: the stringent launch date and the maximum allowable launch mass.

The current launch date in 2026, poses serious constraints and complications to assembly, integration, and verification activities, making it practically unfeasible. It is important to note that the found minima are due to the crossing

Table 22. Mass budget (without launcher adapter)

Subsystem	**Margined mass**
ADCS	62.19 kg
EPS	99.61 kg
GNC	3.52 kg
Mechanisms	29.04 kg
On-board data handling	19.20 kg
Payload	3.50 kg
PS	77.68 kg
STR	63.6 kg
TCS	16.65 kg
TTMTC	16.26 kg
Total	391.25 kg
Total Dry + 20% margin	469.50 kg
Total Wet	525.99 kg

of the ecliptic plane by the asteroids, allowing for the minimum propellant consumption. This event, will not repeat itself in the near future, therefore a different launch date implies an increase in propellant mass.

Preliminary calculations indicate that a local minimum can be found around 2044. The new possible interplanetary trajectory has the following data ranges: launch around July 2044, flyby of `2006 HZ51` in late September or early October 2045, flyby of `2004 QD14` in late February or early March 2046, and rendezvous with `2000 SG344` in June or July 2047. However, this extension of the mission does not respect the requirement to launch before 2030. Additionally, initial estimates suggest that the new propellant mass will be of ∼180 kg.

Acknowledgements

The work presented in this paper has been developed by eleven students over six months in the context of the "Applied Space Mission Analysis and Design" course at Politecnico di Milano. The authors want to acknowledge the other ENEA team members: Haseeb Ashfaq, Martin Degener, Vittoria Gatti, Guglielmo Gomiero, and Filippo Sangiorgi. We would additionally like to thank Andrea Caushi for helping with the trajectory design.

A special thanks is also given to the entire ASTRA Team, for the guidance over the semester. Lastly and most importantly, we wish to express gratitude to Professor Michèle Lavagna who supported and guided the team over the entire project duration.

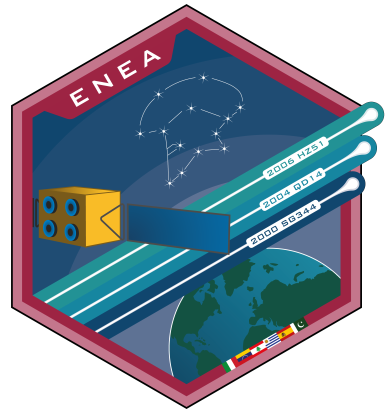

Fig. 7. ENEA mission logo

References

List of references

[1] D. Everett, R. Mink, T. Linn, and J. Wood, "Designing to sample the unknown: Lessons from OSIRIS-REx project systems engineering," 2017.

[2] *DART, impactor spacecraft*. [Online]. Available: `https://dart.jhuapl.edu/Mission/Impactor-Spacecraft.php`.

[3] T. Yoshimitsua *et al.*, "Hayabusa-final autonomous descent and landing based on target marker tracking," *Acta Astronautica*, 2009.

[4] *CREME96*. [Online]. Available: `https://creme.isde.vanderbilt.edu/CREME-MC`.

[5] Marchi, Delbò, Morbidelli, Paolicchi, and Lazzarin, "Heating of near-earth objects and meteoroids due to close approaches to the sun," *Monthly Notices of the Royal Astronomical Society*, 2009.

[6] "Unexpected thermal properties of the near-earth object (499998)," 2011.

[7] W. D. MacMillan, *The Theory of the Potential*. 1930.

[8] J. P. G. William Herbst and T. E. Y. Tetsuo, "The macroporosity of rubble pile asteroid Ryugu and implications for the origin of Chondrules," 2021.

[9] M. J.W., S. D.J., H. S.G., F. D., C. S., and L. D., "The OSIRIS-REx radio science experiment at Bennu," *Springer Nature*, 2018.

[10] R. T. Daly *et al.*, "Shape modeling of Dimorphos for the double asteroid redirection test (DART)," *The Planetary Science Journal*, vol. 3, no. 9, p. 207, Sep. 2022. DOI: `10.3847/psj/ac7523`. [Online]. Available: `https://doi.org/10.3847/psj/ac7523`.

[11] A. PELLACANI, M. GRAZIANO, M. FITTOCK, J. GIL, and I. CARNELLI, "HERA vision based GNC and autonomy," 2019. DOI: 10.13009/EUCASS2019-39. [Online]. Available: https://www.eucass.eu/doi/EUCASS2019-0039.pdf.

[12] J. O. Goldsten, "The NEAR X-ray/Gamma-ray spectrometer," *Johns Hopkins APL Technical Digest*, vol. 19, no. 2, 1998.

[13] F. Jiang, H. Baoyin, and J. Li, "Practical techniques for low-thrust trajectory optimization with homotopic approach," *Journal of Guidance, Control, and Dynamics*, vol. 35, no. 1, pp. 245–258, 2012. DOI: 10.2514/1.52476. eprint: https://doi.org/10.2514/1.52476. [Online]. Available: https://doi.org/10.2514/1.52476.

[14] Y. Wang, F. Topputo, and X. Hou, "Analytic gradients in normalized low-thrust trajectory optimization with interior-point constraints," *Journal of Guidance, Control, and Dynamics*, vol. 47, no. 9, pp. 1980–1990, 2024. DOI: 10.2514/1.G007896. eprint: https://doi.org/10.2514/1.G007896. [Online]. Available: https://doi.org/10.2514/1.G007896.

[15] NASA, JPL, Center for Near Earth Object Studies. "Sentry: Earth impact monitoring." (2024), [Online]. Available: https://cneos.jpl.nasa.gov/sentry/details.html#?des=2000%20SG344.

[16] NASA. "Multilayer insulation material guidelines." (1999), [Online]. Available: https://ntrs.nasa.gov/api/citations/19990047691/downloads/19990047691.pdf.

[17] NASA. "Spacecraft thermal control coatings references." (2005), [Online]. Available: https://core.ac.uk/download/pdf/42754764.pdf.

[18] E. Technologies. "Qioptiq space-qualified coverglass." (2024), [Online]. Available: https://www.excelitas.com/file-download/download/public/58456?filename=Qioptiq_Space-Qualified_Cover_Glass_Datasheet.pdf.

[19] ESA, "Margin philosophy for science assessment studies," 2012. [Online]. Available: https://www.sciencedirect.com/science/article/pii/S009457651300218X.